

Joint inversion of airborne electromagnetic and total magnetic intensity data using Gramian structural constraints: case study of the Reid-Mahaffy test site in Ontario, Canada

Michael Jorgensen*, Leif Cox, and Michael S. Zhdanov, Consortium for Electromagnetic Modeling and Inversion, University of Utah, and TechnoImaging

Summary

Acquisition of airborne electromagnetic (AEM) data is usually combined with the total magnetic intensity (TMI) surveying, making these two geophysical methods a natural choice for joint inversion. In this paper, we present an algorithm for joint inversion of the frequency or time domain airborne electromagnetic (AEM) and TMI data producing structurally similar 3D conductivity and susceptibility models. The method is based on the structural Gramian constraints (Zhdanov et al., 2012; Zhdanov, 2015), which enforce structural correlations of the gradients of different physical property models. The method is illustrated by the results of inverting the frequency-domain DIGHEM AEM and airborne magnetic data collected over the Reid-Mahaffy test site in Ontario, Canada. By combining these complementary datasets, we produce subsurface images of geological structures with the sharper boundaries, stronger structural correlations, and with the same level of data misfit as the standalone inversions.

Introduction

The resolution capability of the AEM method spans depths of several hundred meters and is capable of resolving resistive and conductive targets; however, this nonlinear inverse problem is generally underdetermined, which leads to its non-uniqueness. Joint inversion of multimodal geophysical data can decrease the ambiguity of the inverted physical property models and improve the resolution capability. TMI data is generally gathered in AEM surveys, making the pair a natural choice for joint inversion.

Structural constraints based on model gradients have proven to be an effective tool for joint inversion (Gallardo and Meju, 2003). Our approach to addressing this problem is joint inversion with structural Gramian constraints (Zhdanov et al., 2012; Zhdanov, 2015), which enforce structural correlation of the gradients of different physical property models. As an illustration of this approach, we present the results of inverting the frequency-domain DIGHEM AEM and airborne magnetic data collected over the Reid-Mahaffy test site in Ontario, Canada (Reford and Fyon, 2000). Standalone 1D and 3D inversions are run to determine the general earth structure and to obtain the optimal parameters for the joint inversion. If geologic features, such as conductive overburden, are present and these features are known to be nonmagnetic, the structural enforcement term

in the inversion is spatially limited to a subdomain where the existence of structural correlation is known.

To illustrate the effectiveness of the developed approach, we present the conductivity and magnetic susceptibility models of a subset of the Reid-Mahaffy test site obtained from both standalone and joint Gramian 3D inversions

Theory

We formulate a geophysical inverse problem as a solution of the following operator equations:

$$m^i = (A^i)^{-1} d^i, (i = 1, 2), \quad (1)$$

where m^i are the models, A^i are the forward modelling operators, d^i are the data, and the superscript $i = 1, 2$ indicates the electromagnetic and magnetic problems, respectively.

The regularized solution of inverse problem (1) can be obtained by minimizing the following joint parametric functional:

$$P = \sum_{i=1}^2 \varphi(m^i) + \alpha \sum_{i=1}^2 s(m^i) + \beta G(\nabla m^i) = \min, \quad (2)$$

with a spatially limited Gramian constraint, $G(\nabla m^i)$, and the corresponding misfit functionals,

$$\varphi(m^i) = \|W_d^i (A^i(m^i) - d^i)\|_2^2, \quad (3)$$

where W_d^i are the data weights, $A^i(m^i)$ are the predicted data, and d^i are the observed data. The stabilizing functionals are defined as follows:

$$s(m^i) = \|W_m^i (m^i - m_{apr}^i)\|_2^2, \quad (4)$$

where W_m^i are the model weights, and m_{apr}^i are the a priori models.

The Gramian term, which enforces the structural similarity, is calculated as follows

$$G(\nabla m^i) = \left| \begin{array}{cc} (\nabla m^1, \nabla m^1) & (\nabla m^1, \nabla m^2) \\ (\nabla m^2, \nabla m^1) & (\nabla m^2, \nabla m^2) \end{array} \right|, \quad (5)$$

Gramian joint inversion of AEM and TMI data

where ∇m^i are the gradients of the models, and $(*,*)$ denotes the inner product (Zhdanov, 2015). Minimization problem (2) is solved by the reweighted conjugate gradient method (Zhdanov 2009; 2015).

The regularization parameters, α and β , are adaptively reduced to ensure stable convergence (Zhdanov, 2009; 2015). The inversion is halted when the χ^2 fit corresponding to both misfit terms drops to 1, meaning we have reached the interpreted noise level.

The inversion workflow consists of filtering the TMI data, obtaining a 1D standalone conductivity inverse model to determine depth of conductive overburden, and then obtaining 3D standalone conductivity and susceptibility inverted models for weighting information used in the joint inversion. For areas with strongly conductive overburden, the Gramian constraint is only applied below conductive overburden. This increases the speed of convergence and avoids spurious near surface inhomogeneities in the susceptibility model.

Results

We inverted the data collected over a subdomain of the test site shown in Figures 1 & 2, where the data demonstrated both conductive and magnetic anomalies. The standalone inverted conductivity model (Figure 3) corresponds well to borehole information (Reford and Fyon, 2000) for this target, which indicates conductive overburden to a depth of ~50 m, underlain by layers of intrusive intermediate and felsic rocks and a strongly fractured graphitic ultramafic intrusion. TMI data were filtered to eliminate responses from the deeper sources. Despite filtering, the standalone inverted susceptibility model (Figure 4) resolved a plate like feature at the bottom of the domain, corresponding to a layer of intermediate and felsic volcanics underlying the ultramafic intrusion, complicating interpretation.

We contrast the standalone inverted models with the jointly inverted models (Figures 5 & 6), which have sharper boundaries, more structural correlation, and lack the spurious plate at the bottom of the domain present in the standalone susceptibility model.

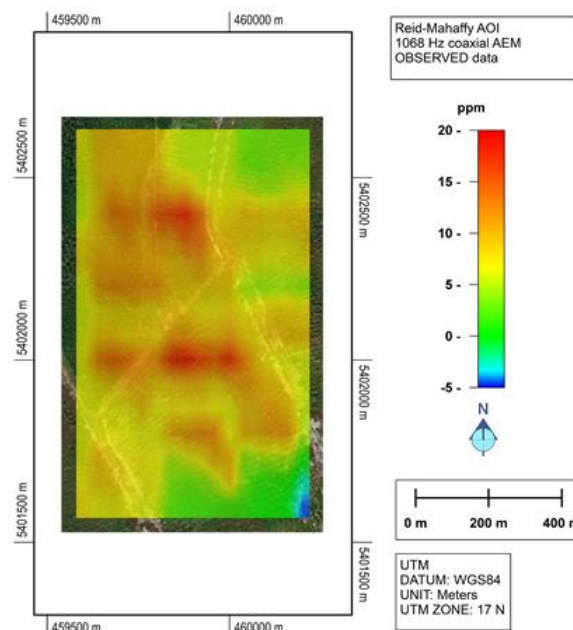


Figure 1: 1068 Hz coaxial DIGHEM observed data map overlaying world imagery.

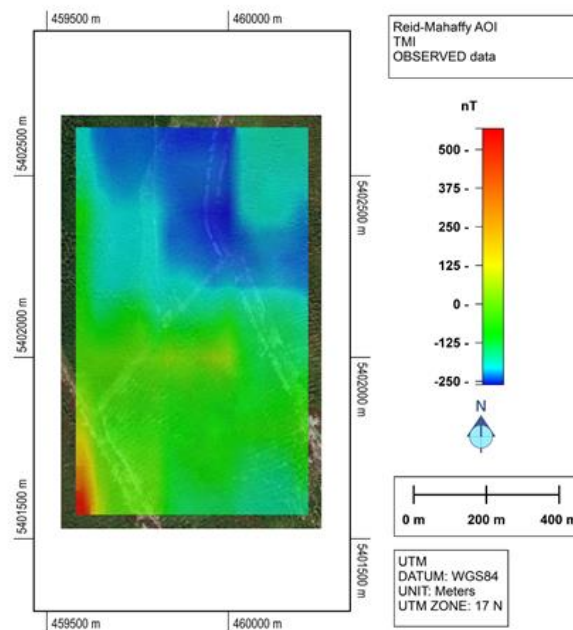


Figure 2: Filtered TMI data map overlaying world imagery.

Gramian joint inversion of AEM and TMI data

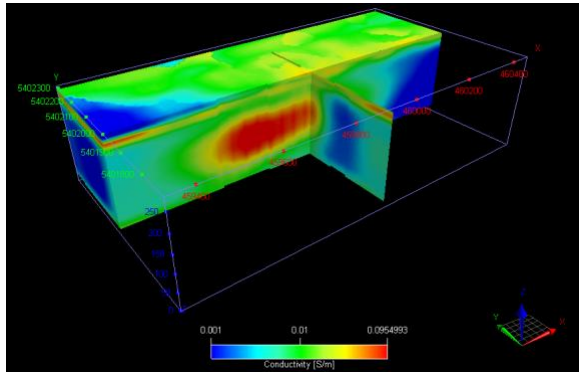


Figure 3: 3D conductivity (S/m) model produced from standalone inversion. Red arrow is easting and green arrow is northing.

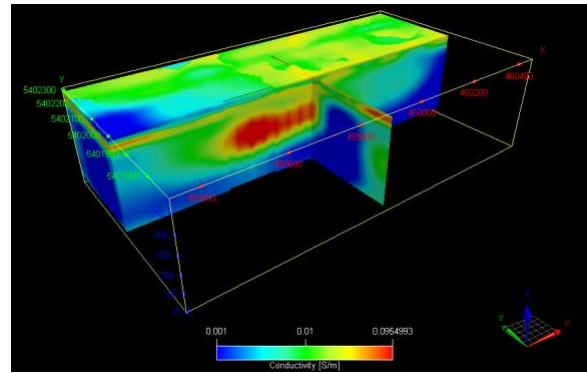


Figure 5: 3D conductivity (S/m) model produced from Gramian joint inversion. Red arrow is easting and green arrow is northing.

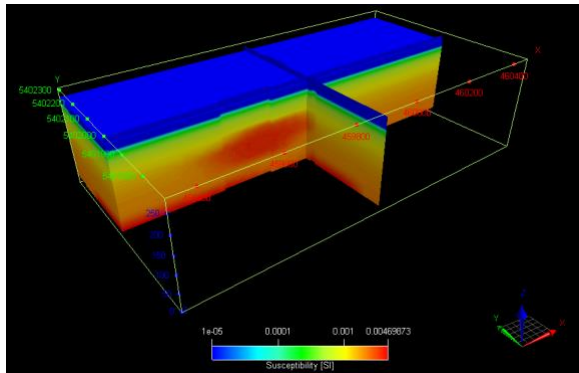


Figure 4: 3D susceptibility (SI) model produced from standalone inversion. Red arrow is easting and green arrow is northing.

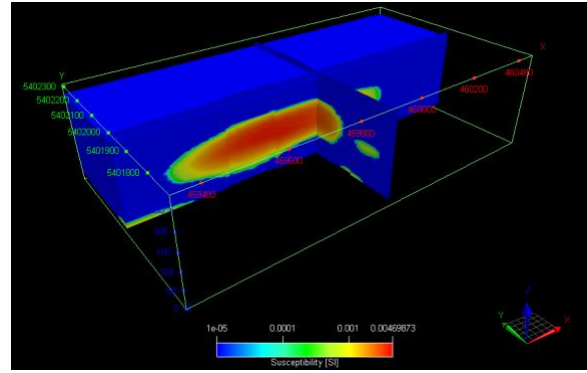


Figure 6: 3D susceptibility (SI) model produced from Gramian joint inversion. Red arrow is easting and green arrow is northing.

Figures 7 & 8 compare the observed and predicted data fits for both the standalone and Gramian joint inversions, respectively. It is important to note the same level of data misfit is achieved by both methods.

The cross plots of susceptibility and log conductivity shown in Figure 9 indicate the level of structural correlation. The nebulous cloud representing the standalone inverted models indicates minimal correlation, making interpretation difficult. Conversely, the parabolic trend representing the jointly inverted models, combined with sharper geospatial boundaries and target coincidence, can significantly ease interpretation.

Conclusions

We have introduced a method of joint inversion of AEM and TMI data using Gramian structural constraints. We have jointly inverted frequency-domain DIGHEM and airborne magnetic data gathered over the Reid-Mahaffy test site. Comparison of the standalone inverted resistivity and susceptibility models versus the joint inverted models, which all have the same level of data misfit ($\chi^2 = 1$), demonstrates that the jointly inverted models can recover the more compact bodies, more structural correlation, and more geologically reasonable models than the standalone inverse solutions.

Acknowledgements

The authors would like to thank Consortium for Electromagnetic Modeling and Inversion (CEMI) at the University of Utah and Technomaging for their support. The AEM and TMI data were collected by Fugro and made available by the Ontario Geological Survey, Canada.

Gramian joint inversion of AEM and TMI data

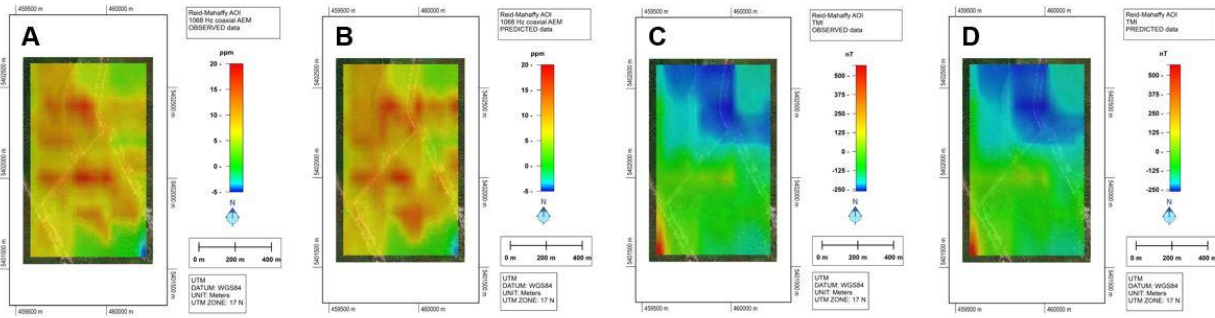


Figure 7: Panels A & B show observed and predicted AEM data produced by standalone inversion, respectively, for the 1068 Hz coaxial component, which is most sensitive to the conductive mineralization. Panels C & D show observed and predicted TMI data produced by standalone inversion, respectively.

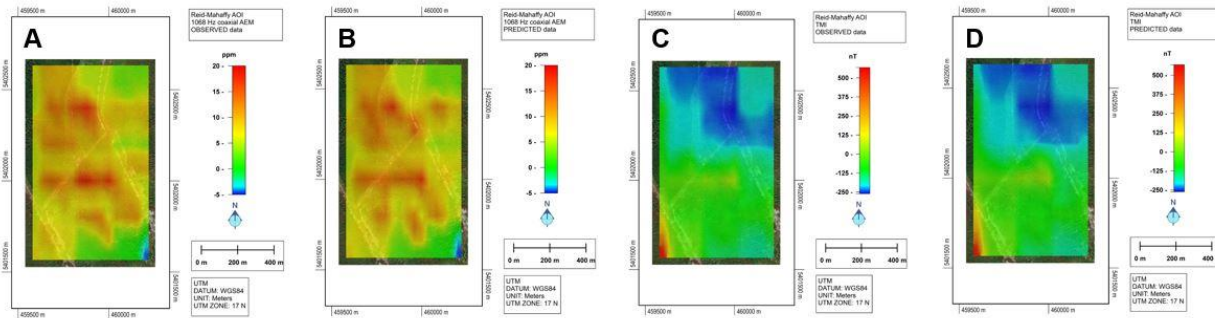


Figure 8: Panels A & B show observed and predicted AEM data produced by Gramian joint inversion, respectively, for the 1068 Hz coaxial component, which is most sensitive to the conductive mineralization. Panels C & D show observed and predicted TMI data produced by Gramian joint inversion, respectively.

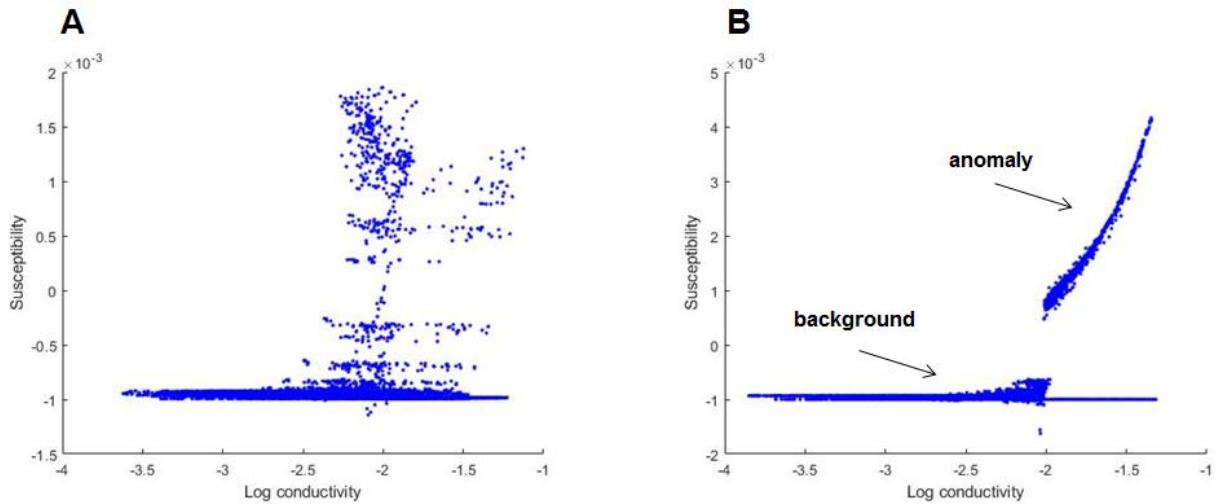


Figure 9: Panels A & B show property cross plots of susceptibility and log conductivity for the standalone inverted models and jointly inverted model, respectively. The jointly inverted models show enhanced structural correlation of the target.

REFERENCES

- Gallardo, L. A., and M. A. Meju, 2003, Characterization of heterogeneous near-surface materials by joint 2D inversion of DC resistivity and seismic data: *Geophysical Research Letters*, **30**, 1658, doi: <https://doi.org/10.1029/2003GL017370>.
- Reford, S. W., and A. Fyon, 2000, Airborne magnetic and electromagnetic surveys, Reid-Mahaffy airborne geophysical test site survey, miscellaneous release—Data (MRD) 55, geological setting, measured and processed data, and derived products: Published report. <http://www.geologyontario.mndm.gov.on.ca/mndmfiles/pub/data/imaging/MRD055/MRD055.pdf>.
- Zhdanov, M. S., 2009, *Geophysical electromagnetic theory and methods*: Elsevier.
- Zhdanov, M. S., 2015, *Inverse theory and applications in geophysics*: Elsevier.
- Zhdanov, M. S., A. V. Gribenko, and G. Wilson, 2012, Generalized joint inversion of multimodal geophysical data using Gramian constraints: *Geophysical Research Letters*, **39**, doi: <https://doi.org/10.1029/2012GL051233>.